Characterization of mesoscale gravity waves in the upper and lower clouds of Venus from VEX-VIRTIS images

Javier Peralta, R. Hueso, Agustín Sánchez-Lavega, Giuseppe Piccioni, O. Lanciano, Pierre Drossart

Characterization of mesoscale gravity waves in the upper and lower clouds of Venus from VEX-VIRTIS images

J. Peralta,[1] R. Hueso,[1] A. Sánchez-Lavega,[1] G. Piccioni,[2] O. Lanciano,[2] and P. Drossart[3]

Received 9 May 2008; revised 11 August 2008; accepted 22 August 2008; published 11 December 2008.

[1] Images obtained from the Visible and InfraRed Thermal Imaging Spectrometer (VIRTIS)-M instrument onboard Venus Express present visible trains of alternating bands of cloud brightness in two different layers: at the upper cloud tops (~66 km altitude) observed in the dayside hemisphere using reflected ultraviolet light (380 nm) and in the lower cloud (~47 km altitude) observed in the nightside hemisphere using thermal radiation (1.74 μm). The waves are nearly zonal (with the bands perpendicular to latitude circles), have wavelengths of 60–150 km, propagate westward with low phase velocities relative to the zonal flow, and are confined in wave packets of 400 to 1800 km in length. The waves in the lower cloud observed in the infrared are widely distributed around the planet, and their appearance varies widely throughout the VIRTIS data set. The locations of both types of waves seem not correlated with latitude, local times, surface topography, or the structure of the wind. In both cases the characteristics of the waves correspond to gravity waves propagating in confined stable layers of the atmosphere. We examine the properties of these waves in terms of a linear model and perform a simple analysis to discuss the vertical stability of the atmosphere within Venus clouds.

Citation: Peralta, J., R. Hueso, A. Sánchez-Lavega, G. Piccioni, O. Lanciano, and P. Drossart (2008), Characterization of mesoscale gravity waves in the upper and lower clouds of Venus from VEX-VIRTIS images, *J. Geophys. Res.*, *113*, E00B18, doi:10.1029/2008JE003185.

1. Introduction

[2] Atmospheric internal gravity waves are wave disturbances whose restoration force is buoyancy under stable stratification of the atmosphere [*Holton*, 1992]. They are commonly observed in the stratosphere of most planets as oscillations on the temperature field and they have also been observed as wavy structures in cloud fields of the Earth [*Houze*, 1993], Jupiter [*Hunt and Muller*, 1979; *Flasar and Gierasch*, 1986; *Reuter et al.*, 2007] and Venus [*Gierasch et al.*, 1997; *Markiewicz et al.*, 2007]. Since they are supported by such a fundamental force (buoyancy) they are of great interest to atmospheric dynamics. On the one hand, from their properties one can infer the static stability of the atmosphere (since these waves can only propagate in regions where the static stability is positive). On the other, they are responsible of a number of important dynamical phenomena including the transfer of energy and momentum vertically. They are of particular importance to the atmosphere of Venus, where their role as a mechanism able to transport momentum from the surface to the atmospheric mean circulation has been examined by several teams, although without a final consensus on their role in powering the atmospheric superrotation [*Hou and Farrell*, 1987; *Gierasch*, 1987; *Leroy and Ingersoll*, 1995]. Space probes determined during their descent at different latitudes and local times the existence of at least two stable layers: between 30 and 48 km, and upward of 55 km [*Kliore and Patel*, 1980; *Seiff et al.*, 1985; *Gierasch*, 1987]. These altitude levels are home to dense clouds on Venus [*Esposito et al.*, 1997] and gravity waves arising on them can manifest as regular patterns on the clouds albedo fields [*Markiewicz et al.*, 2007; *McGouldrick and Toon*, 2008]. The altitudes below 30 km and the intermediate layer between 48 and 55 km have small static stabilities and are not suitable candidates for the development of gravity waves.

[3] Gravity waves observed at the upper cloud level were first inferred from analysis of Mariner 10 [*Belton et al.*, 1976] and Pioneer Venus [*Rossow et al.*, 1980] ultraviolet images of the upper cloud field at z ~ 65 km. More recently, the Venus Monitoring Camera (VMC) onboard Venus Express has also detected regular cloud patterns identified as gravity waves from their observed characteristics [*Markiewicz et al.*, 2007]. Mariner 10 images of equatorial elongated cloud patterns of about 5000 km in the longitudinal direction and separated ~500 km in latitude (circumequatorial belts) were interpreted as evidence of internal gravity waves. These structures propagated southward near the equator with phase speeds of ~20 m/s [*Belton et al.*, 1976]. The same circumequatorial belts were seen during the Pioneer Venus mission in addition

[1] Departamento de Física Aplicada I, Escuela Técnica Superior de Ingenieríos, Universidad del País Vasco, Bilbao, Spain.
[2] Istituto di Astrofisica Spaziale e Fisica Cosmica, Istituto Nazionale di Astrofisica, Rome, Italy.
[3] Laboratoire d'Etudes Spatiales et d'Instrumentation en Astrophysique, Observatoire de Paris, UPMC, Université Paris-Diderot, CNRS, Meudon, France.

0148-0227/08/2008JE003185

to a new type of train of wavelike features composed of dark streaks of ~2000 km, separated by ~200 km, but in this case lying at a large angle to the constant latitude circles [*Rossow et al.*, 1980]. No evidence for small-scale internal gravity waves or for circumequatorial belts was found in images taken by the Galileo spacecraft in 1990 [*Belton et al.*, 1991; *Toigo et al.*, 1994; *Peralta et al.*, 2007a]. This was linked to a lower abundance of convective clouds visible during the Galileo flyby. The high-resolution images obtained recently by the VMC instrument onboard Venus Express display vigorous convection in near equatorial latitudes and visible wave activity (wavelengths of just a few tens of kilometers) in tropical latitudes in the south hemisphere and in middle to subpolar latitudes in the north hemisphere [*Markiewicz et al.*, 2007].

[4] Evidence for gravity waves in the Venus atmosphere does not come only from imagery. The four Pioneer Venus probes, as they descended through the atmosphere, obtained altitude profiles of temperature (upward of 110 km) and wind velocity (lower cloud region) that showed wavelike variations with vertical wavelengths of 5–10 km [*Seiff at al.*, 1980; *Counselman et al.*, 1980]. Similar vertical variations can be seen in infrared temperature soundings [*Taylor et al.*, 1980], and in radio occultation temperatures from Pioneer Venus [*Kliore and Patel*, 1980], Venera 9 [*Kolosov et al.*, 1980] and Magellan [*Hinson and Jenkins*, 1995] sensitive to mesospheric vertical levels between the cloud tops ($z \sim 65$ km) and the thermosphere base ($z \sim 100$ km). Above these levels, gravity waves with wavelengths between 100 and 600 km have also been detected on the thermosphere as density perturbations studied by the mass spectrometer on the Pioneer Venus orbiter [*Niemann et al.*, 1980; *Kasprzak et al.*, 1988], and from non LTE CO_2 emissions observed by the Visible and InfraRed Thermal Imaging Spectrometer (VIRTIS) instrument on Venus Express (R. García et al., Gravity waves in Venus upper atmosphere revealed by CO_2 non LTE emissions, submitted to *Journal of Geophysical Research*, 2008).

[5] Although several candidates could act as sources of gravity waves (flow over a mountain range, Kelvin-Helmholtz instability around a jet stream), convective processes generated in the low-stability layers between 48 and 55 km and below 30 km are considered to play the main role for gravity wave generation in the middle and upper regions of the clouds layer [*Schubert*, 1983; *Gierasch*, 1987; *Leroy and Ingersoll*, 1995, 1996; *Baker et al.*, 2000a, 2000b].

[6] In this paper we present the observed characteristics of wavelike features present in the atmosphere of Venus at two cloud levels detected on images at different wavelengths obtained by the VIRTIS instrument [*Drossart et al.*, 2007] onboard Venus Express [*Svedhem et al.*, 2007]. We identify these features as gravity waves and present a simple theoretical approach to interpret them in terms of a "textbook" classical linear model. This is the first time that the abundant and variable mesoscale gravity waves within the lower cloud level of Venus have been characterized. From the comparison between the observations and model we infer the existence of a widely (from latitudes 40° to 80°S) and temporarily extended vertical stable region between 30 and 48 km, in agreement with previous inferences [*Gierasch*, 1987; *Leroy and Ingersoll*, 1995].

2. Observations

[7] The instrument VIRTIS on board Venus Express is an imaging spectrometer (VIRTIS-M) combined with a high-resolution IR-spectrometer (VIRTIS-H). VIRTIS-M is capable of obtaining images over several visible and infrared wavelengths in two channels: visible (0.3 to 1 μm) and near infrared (1 to 5 μm) [*Drossart et al.*, 2007]. Dayside observations in the ultraviolet show cloud features in the upper cloud (380 nm), corresponding to an altitude of ~(66 ± 4) km. At the near infrared 980 nm, solar photons are more penetrating and reach the base of the upper cloud at ~(61 ± 3) km [*Belton et al.*, 1991; *Peralta et al.*, 2007b]. Night side images of Venus at 1.74 μm are sensitive to the opacity of the lower cloud layer at ~44–48 km, with the radiance coming from altitude levels beneath the clouds and being attenuated as it passes through the lower cloud layer [*Carlson et al.*, 1991; *Crisp et al.*, 1991]. *Sánchez-Lavega et al.* [2008] present a detailed account of the global cloud dynamics observed in these filters and the relation between wavelength and cloud altitude determination.

[8] Because of the highly elliptical orbit of the VEX spacecraft, with nearly 80°N pericenter, only the south hemisphere can be covered by the VIRTIS instrument. The spatial resolution of VIRTIS images vary from 15 km/pix at polar and subpolar latitudes to 45 km/pix at equatorial latitudes. The nightside images used in this study cover the period from 12 April 2006 (Orbit Insertion) to 9 March 2007. The dayside images cover the period from Orbit Insertion to 28 July 2007, extending during a large fraction of the nominal mission. The examined period for the visible images was extended compared to the infrared images because of the lower number of orbits containing high-resolution well-contrasted images of the dayside. From these periods, and attending to image quality and spatial resolution, we selected observations corresponding to 112 orbits in the visible and 116 orbits in the infrared.

[9] Figure 1 shows maps of the number of observations for each latitude and local time with a high spatial resolution suitable for gravity waves search (spatial resolution better than 30 km/pix). This roughly corresponds to latitudes poleward of 30°S in both day and nightside.

[10] The images were navigated, corrected from defects (mainly striations and hot and dark lines), processed and mapped into cylindrical and polar projections using the "Planetary Laboratory Image Analysis" (PLIA) software (R Hueso et al., The Planetary Laboratory for Image Analysis (PLIA), submitted to *Planetary and Space Science*, 2008.). Each image was processed individually by a combination of contrast enhancement, unsharp mask and smoothing filters.

3. Results

[11] Examples of systems of waves observed in the cloud fields in ultraviolet (380 nm), near-infrared (980 nm) and infrared (1.74 μm) wavelengths (hereafter, UV, NIR and IR,

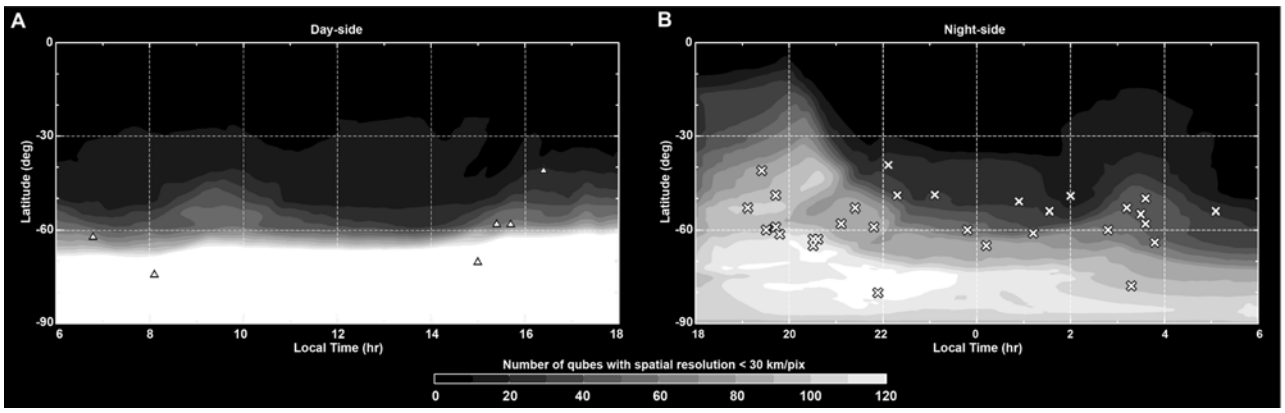

Figure 1. Global resolution maps and frequency of high-resolution observations made with Visible and InfraRed Thermal Imaging Spectrometer (VIRTIS) on the (a) dayside and (b) nightside of Venus. The number of observations of a specific latitude-local time with a high spatial resolution of 30 km/pix is indicated. This spatial resolution is suitable for observations of waves with wavelengths larger than ~100 km. Observations with better resolutions of the order of 15–20 km/pix were also present in the data set with much less frequency. The position of the waves encountered is shown as symbols (triangles for the waves in the upper cloud, and crosses for the waves in the lower cloud) and correlates with regions with high number of observations at this resolution.

respectively) are displayed in Figure 2. The spatially distributed regular patterns of alternative bright and dark stripes represent reflectivity variations in the ultraviolet and near infrared (observed during dayside) and opacity variations in the infrared (observed during nightside). The images show trains of crests and troughs generally ordered in longitude (oriented in the zonal direction) and extending a few degrees in latitude nearly perpendicularly to the wave packet. In many cases the troughs are wider than the crests, or they simply disappear. Some of the wave packets are very regular while others have nonequidistant crests, change their latitudinal dimensions over the packet or show a slight curvature. Beside on Venus, these irregularities have also been observed in mesoscale cloud waves observed in Jupiter and interpreted in terms of ducted gravity waves [*Flasar and Gierasch*, 1986].

[12] We performed a systematic search of waves (see Figure 1) as those shown on Figure 2, finding 6 distinctive and separate wave packets in ultraviolet images, one wave packet in the near infrared (this wave system was observed simultaneously in the ultraviolet and the infrared with nearly identical characteristics) and 30 wave packets in infrared images. In some cases, a single infrared image presents wave systems at various latitudes. The larger abundance of waves in the infrared images results in a larger diversity of wave properties. The average image contrast variations that characterize these wave systems are on the order of 1% in the ultraviolet, less than 1% in the near infrared and vary widely in the infrared with some faint wavy structures with contrast variations of 1%, subtle to detect, to clearly observable systems with contrast of 15%. This study does not rule out the possible existence of less conspicuous wave variations in the cloud fields with less contrast or shorter wavelengths as found in the upper cloud by the VMC instrument [*Markiewicz et al.*, 2007].

[13] We measured the observable properties of the wave packets such as their latitude and local time location, packet length (i.e., their extension perpendicular to the wavefronts), packed width (i.e., their extension in the wavefront direction) and orientation respect to the parallels (lines of constant latitude). Results are listed in Tables 1a–1c.

[14] Figure 3 shows the location of the clouds in terms of latitudes, local times and surface topography. These maps show abundant waves at the lower cloud with no correlation in their position with surface topography (Figure 3a) or local time (Figure 3b). This is in contrast to the northern hemisphere, where the Vega balloon registered the influence of the surface in atmospheric motions with oscillations at the lower cloud level interpreted as gravity waves generated by the flow over specific mountainous regions [*Sagdeev et al.*, 1986; *Young et al.*, 1987, 1994]. In the southern hemisphere, where the surface is nearly flat compared to the northern hemisphere, especially in the sampled latitudes, the waves seem to be present all along the nightside hemisphere except inside the South Polar Dipole [*Piccioni et al.*, 2007]. This could be due to an observational effect since the dipole interior is particularly dark on the infrared images. In any case, gravity waves have been detected up to the dipole's outer edge (80°S in orbit 84) and the global dynamics of the polar area will be presented elsewhere.

[15] The Venus Monitoring Camera on VEX has found abundant cloud waves of higher frequency (wavelengths of a few tens of km) in the upper clouds from south tropical to north polar latitudes [*Markiewicz et al.*, 2007]. These waves, if also present in the south hemisphere, cannot be resolved by VIRTIS observations. The scarcity of large waves detected on the upper clouds does not allow extracting a clear conclusion about their distribution but they seem clustered in the early morning hours and late afternoon. In both cloud layers, we do not find wave packets equatorward of 40°S. This is probably caused by the comparatively low number of high-resolution observations of those latitudes. However, we would also like to point out that at those latitudes there seems to be a transition to different cloud structures, with dark midlatitude bands in the upper cloud (UV), and a mottled turbulent morphology in the lower

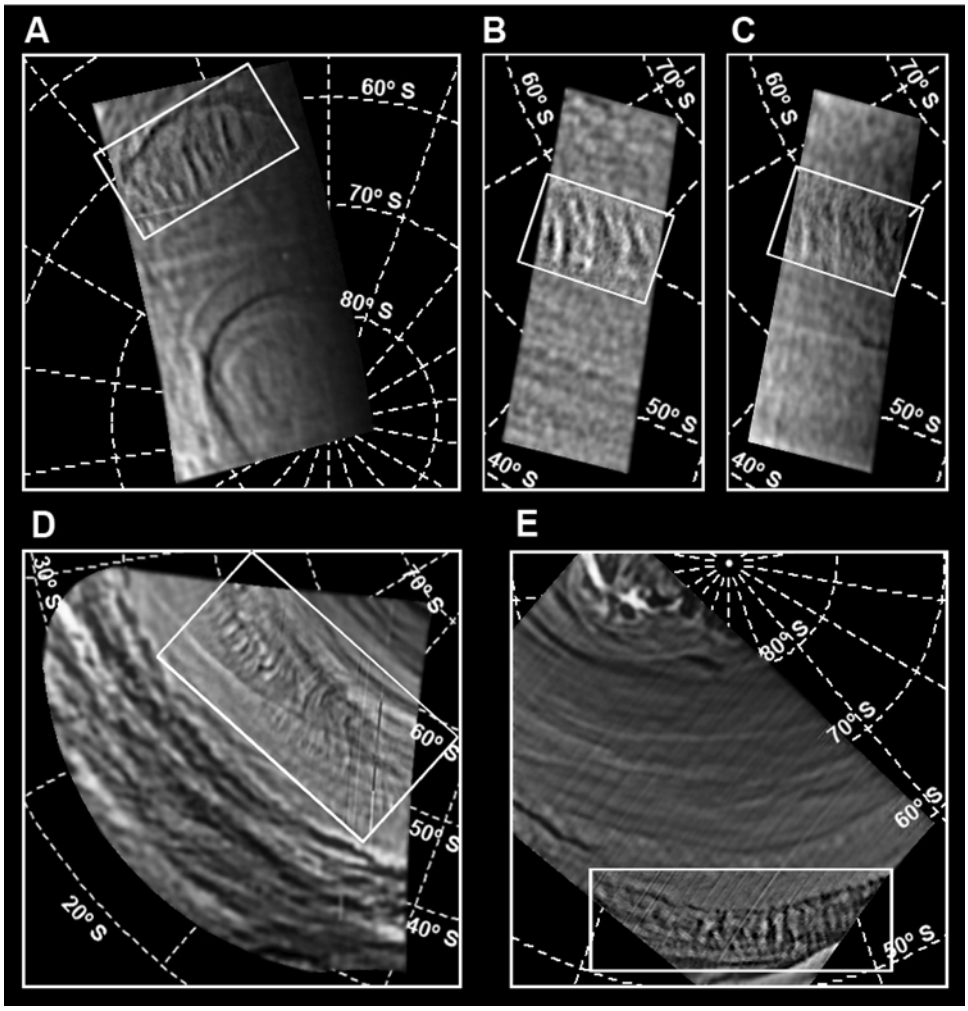

Figure 2. Examples of cloud waves observed on VIRTIS images projected into polar maps for size comparison. Figures 2a and 2b show waves observed at 380 nm in the upper cloud level. The singular detection of a wave at 980 nm images is shown in Figure 2c and correlates with the same structure observed in 380 nm and shown in Figure 2b. Either this is a vertically extended wave, or the observed levels in those wavelengths can be closer than expected at specific latitudes. Large wave packets observed in 1.74 μm in the lower cloud are shown in Figures 2d and 2e.

cloud (IR) that on the one hand may difficult the detection of gravity waves but could also represent a region of active cellular convection where gravity waves might not be generated.

[16] The extension covered by the wave packets, i.e., the packet length, varies between 640 and 1200 km in the upper cloud (UV) with a mean value of 920 km and from 280 to 1700 km in the lower cloud (IR) with a mean value of 760 km. Their average width are 320 and 230 km in the in the upper (UV) and lower cloud (IR), respectively. We further measured the wavelength of each packet, the number of crests and, when possible, their zonal motions. Since the winds at cloud level derived from VIRTIS are variable in terms of the local time [*Sánchez-Lavega et al.*, 2008] we also measured the local velocity at nearby longitudes and latitudes of each individual wave packet to better estimate their phase speed relative to the local wind. This was done only on those orbits where we could observe the same cloud

Table 1a. Summary of Wave Packets Properties From UV Images by VEX-VIRTIS[a]

Orbit	Date (mm/dd/yy)	Latitude (deg)	Local Hour	Packet Length (km)	Packet Width (km)	Orientation (deg)
59	06/18/2006	−41	16,4	>860	170	25
59	06/18/2006	−58	15,7	>865	340	30
170	10/07/2006	−62	06,8	1275	340	25
255	12/31/2006	−70	15,0	980	420	40
388	05/13/2007	−74	08,1	640	335	2

[a]Visible and InfraRed Thermal Imaging Spectrometer (VIRTIS).

Table 1b. Summary of Wave Packets Properties From NIR Images by VEX-VIRTIS

Orbit	Date (mm/dd/yy)	Latitude (deg)	Local Hour	Packet Length (km)	Packet Width (km)	Orientation (deg)
59	06/18/2006	−58	15.4	>860	350	35

field with time differences large enough to track the motions (1 h). Repeated observations of the same wave features indicate they conserve their morphology and albedo variations over these timescales being nondispersive. These properties appear detailed in Tables 2a–2c.

[17] Observed wavelengths are within the range of 90 to 170 km in the upper cloud (UV) and 60 to 180 km in the lower cloud but we cannot rule out waves of higher frequencies (wavelengths shorter than 50 km) not resolved by our observations. At both cloud levels the phase velocities turn out to be generally low respect to the averaged zonal flow. This is in agreement with our interpretation in terms of gravity waves that will be later discussed.

[18] The overall properties of these wave systems do not seem to vary with latitude or local time. The wavelength behavior and wave packet properties in terms of latitude appear on Figure 4. Neither the wavelength (Figure 4a), nor the wave packet length (Figure 4b) or the wave packet width (Figure 4b) seem to be correlated with latitude. Only the wave packet orientation (Figure 4d) seems to slightly grow at higher (more poleward) latitudes. The wave system detected on the outer edge of the dipole is aligned with this structure and presents the largest inclination with respect to the parallels.

[19] The derivation of the properties detailed above critically depends on the quality of the data and, for the determination of the wavelengths and phase speeds, in the ability to accurately track specific structures in the wavefronts and outside them. We estimate the navigation error to be lower than 1 pixel but since all the measurements were done by a human operator the measurement error can be larger. We therefore estimate the wavelengths to be accurate to a 10%, packet lengths and widths accurate to a few tens of km and phase speeds to have a mean measurement error of 8 m/s. The sometimes subtle identification of wave patterns in ultraviolet images relied on the confirmation of all wave structures by a second operator.

4. Discussion

[20] On the basis of the characteristics of the wave systems described above we interpret them as internal gravity waves lying at regions of positive static stability. On the one hand, the high frequency of the waves and the slow rotation of the planet discard the observed waves as manifestations of Rossby waves and on the other, these frequencies are much smaller than the acoustic cut-off frequency. Also their latitudes and short sizes discard Kelvin waves as the underlying mechanism for the regular cloud patterns. Roll convection on Earth sometimes produces structures similar in their shape to the regular alignment of clouds observed on our images but this phenomenon is characteristic of the planetary boundary layer and depends on a critical equilibrium between a small static stability and

Table 1c. Summary of Wave Packets Properties From IR Images by VEX-VIRTIS

Orbit	Date (mm/dd/yy)	Latitude (deg)	Local Hour	Packet Length (km)	Packet Width (km)	Orientation (deg)
84	07/13/2006	−80	21,9	>600	225	50
96	07/25/2006	−48	02,0	1750	520	15
97	07/26/2006	−39	22,1	660	160	35
97	07/26/2006	−61	19,8	570	160	40
100	07/29/2006	−55	03,5	>1525	270	2
112	08/10/2006	−60	23,8	610	105	20
112	08/10/2006	−49	23,1	410	170	40
112	08/10/2006	−49	22,3	730	320	25
112	08/10/2006	−53	21,4	785	200	8
112	08/10/2006	−58	21,1	575	205	7
113	08/11/2006	−54	01,5	>1140	180	17
114	08/12/2006	−54	05,1	>645	205	14
118	08/16/2006	−65	00,2	635	265	2
141	09/08/2006	−65	20,5	520	370	11
142	09/09/2006	−64	03,8	>1415	160	13
161	09/28/2006	−58	03,6	1050	310	17
164	10/01/2006	−50	03,6	335	380	20
166	10/03/2006	−53	03,2	>790	225	12
228	12/04/2006	−51	00,9	690	370	10
231	12/07/2006	−78	03,3	280	130	30
261	01/06/2007	−59	21,8	620	240	13
290	02/04/2007	−63	20,6	>440	250	4
313	02/27/2007	−60	02,8	>860	315	11
315	03/01/2007	−61	01,2	760	335	0
317	03/04/2007	−53	19,1	>1230	170	10
317	03/04/2007	−59	19,7	685	200	15
317	03/04/2007	−63	20,5	450	145	7
318	03/05/2007	−60	19,5	640	150	0
321	03/07/2007	−49	19,7	>1300	210	12
323	03/10/2007	−41	19,4	615	200	0

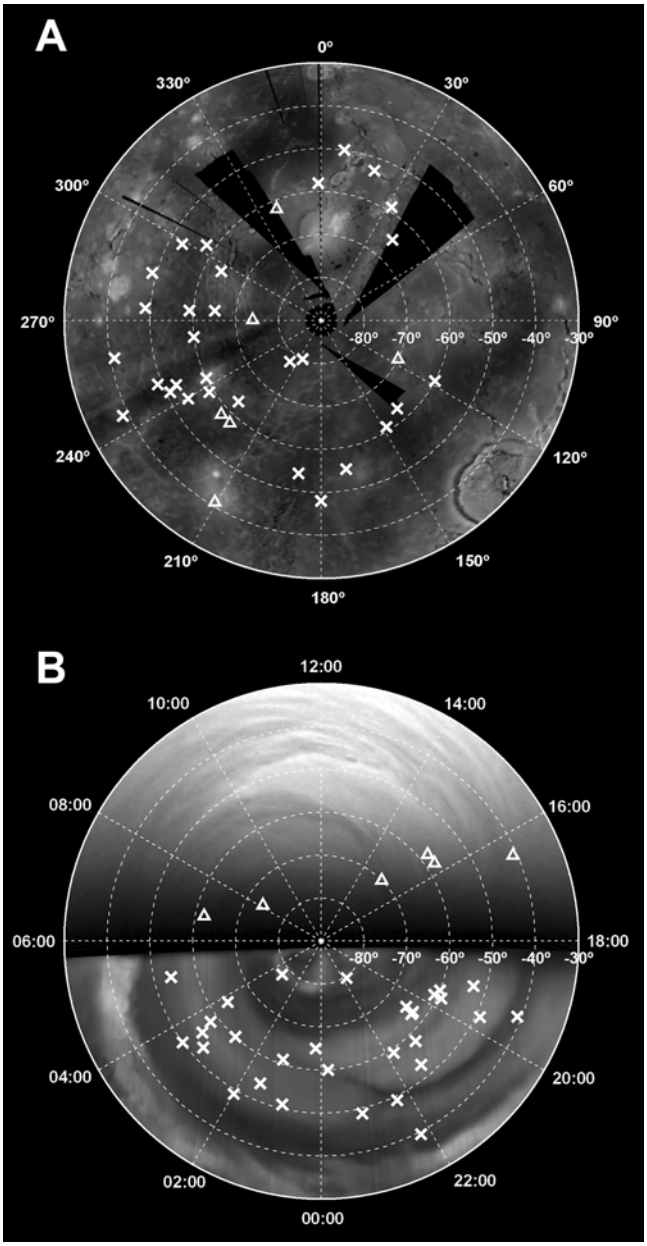

Figure 3. Polar map of cloud waves' locations in terms of their longitude, local time, morphology of the clouds, and surface topography. Figure 3a shows the wave packets central positions (triangles for the waves in the upper cloud, and crosses for the waves in the lower cloud) over a surface map obtained by the Magellan IDRS instrument [*Saunders et al.*, 1991]. The topography varies from −1.3 km in the darkest low plains to +2.5 km at the top of the highest mountains in this projection. The higher concentration of waves in the sector between longitudes 210–300° is due to a bias in the spatial sampling. Figure 3b shows the cloud waves in terms of latitude and local time displaying the typical cloud structure at these levels with a background image from the Venus Orbit Insertion covering the whole southern hemisphere. Given the spatial resolution and sampling of the polar region, the lack of cloud waves at these latitudes might be significant.

Table 2a. Summary of Wave Properties From UV Images by VEX-VIRTIS

Orbit	Latitude (deg)	Number of Crests	Wave Length (km)	Crest Width (km)	c_x (m/s)	$\lvert\vec{c}\rvert-\bar{u}$ (m/s)
59	−41	8	95	45	−113	−12
59	−58	7	115	60	−108	−40
170	−62	5	210	125	−62	0.5
255	−70	11	90	45	−29	14
388	−74	4	170	100	−76	−36

a dynamic instability due to the vertical wind shear (low values of the Richardson number). Our wave systems are located several tens of km above the surface and at regions of high Richardson numbers.

[21] In order to gain insight into the nature of the waves and further determine their characteristics, we will examine their wave dispersion relation using a simple "textbook" classical linear model of gravity waves. The wave dispersion relation can be deduced by neglecting the effects of rotation under the Boussinesq approximation and assuming two-dimensional motion. Linear perturbations over a basic state with constant zonal flow and density yield the dispersion relation [*Holton*, 1992]:

$$(\omega - \bar{u}k)^2 = \frac{k^2}{k^2 + m^2} N^2, \tag{1}$$

where ω is the frequency of the wave perturbation, $\bar{u}$ is the mean wind projected in the direction of the wave phase propagation, N^2 is the square of the buoyancy or Brunt-Väisällä frequency, and k and m are the horizontal and vertical wave numbers related to the horizontal and vertical wavelengths, λ_x and λ_z, by $k = 2\pi/\lambda_x$ and $m = 2\pi/\lambda_z$. From (1) it is straightforward to deduce the horizontal and vertical components of the phase speed vector relative to the mean flow as,

$$c_x = \pm \frac{N}{\sqrt{k^2 + m^2}} \tag{2a}$$

$$c_z = \pm \frac{N}{\sqrt{k^2 + m^2}} \frac{k}{m}, \tag{2b}$$

where c_x is the phase speed relative to the mean wind flow. We now proceed to verify if those waves for which we have information about their phase speeds verify this simple model of internal gravity waves.

[22] The clouds observed in the ultraviolet are located at ~66 km altitude. These levels are close to the transition between the troposphere and the mesosphere, where the static stability of the atmosphere abruptly increases. A reasonable value of the Brunt-Väisälä frequency from

Table 2b. Summary of Wave Properties From NIR Images by VEX-VIRTIS

Orbit	Latitude (deg)	Number of Crests	Wave Length (km)	Crest Width (km)	c_x (m/s)	$\lvert\vec{c}\rvert-\bar{u}$ (m/s)
59	−58	7	125	75	-	-

Table 2c. Summary of Wave Properties From IR Images by VEX-VIRTIS

Orbit	Latitude (deg)	Number of Crests	Wave Length (km)	Crest Width (km)	c_x (m/s)	$\lvert\vec{c}\rvert-\bar{u}$ (m/s)
84	−80	6	63	40	−26	−1.0
96	−48	12	155	70	−64	−9.0
97	−39	8	100	35	−59	−3.1
97	−61	8	80	30	−58	−2.7
100	−55	12	130	65	-	-
112	−60	8	60	30	-	-
112	−49	5	103	50	-	-
112	−49	7	90	20	-	-
112	−53	6	125	70	-	-
112	−58	4	105	45	-	-
113	−54	6	140	90	-	-
114	−54	5	100	40	-	-
118	−65	7	90	50	-	-
141	−65	4	180	75	−44	−0.2
142	−64	18	75	44	-	-
161	−58	14	75	40	−61	−5.1
164	−50	4	100	50	−64	−1.8
166	−53	6	130	60	-	-
228	−51	5	130	65	−45	−29.7
231	−78	5	105	65	-	-
261	−59	4	145	65	−42	9.0
290	−63	4	120	66	-	-
313	−60	7	135	65	−60	5.0
315	−61	6	100	55	−64	3.1
317	−53	9	100	55	−59	2.4
317	−59	9	90	50	−60	1.1
317	−63	6	90	45	−66	−6.1
318	−60	5	100	50	−54	−7.5
321	−49	12	105	50	-	-
323	−41	5	110	55	−50	3.3

different probes for these levels is $N^2 \approx 260 \cdot 10^{-6}$ s^{-2} [*Seiff et al.*, 1985; *Del Genio and Rossow*, 1990; *Gierasch et al.*, 1997]. Above these levels the stability of the atmosphere increases to higher values characteristic of the mesosphere. Below the clouds the stability decreases to nearly zero allowing for a region between 48 and 55 km where vertical convection can develop. The lower clouds acting as a source of opacity for the atmospheric emitted radiation are located just below, in altitudes (43–48 km) characterized by high values of the static stability. We consider as a representative value for the Brunt-Väisälä frequency in the lower cloud $N^2 \approx 65 \cdot 10^{-6}$ s^{-2}. This is close to the peak values measured by the Pioneer Venus Night Sounder at the height of 45 km [*Seiff et al.*, 1985; *Gierasch et al.*, 1997] over the stable layer situated in the height range 30–48 km, and it is within the range of 50–$100 \cdot 10^{-6}$ s^{-2} obtained at these altitudes by the ensemble of Pioneer Venus sounders. This stable layer may act as a duct where waves can form excited by convection from the lower levels or from downdrafts from the unstable levels above [*Baker et al.*, 1998].

[23] Figure 5 shows the behavior of the gravity wave dispersion relationship for different values of the vertical wavelength λ_z and the assumed values of the Brunt-Väisälä frequency. The upper cloud waves (Figure 5a) seem to be distributed in two groups of short (5 km) and large (15 km) vertical wavelengths or in regions with small and large values of the atmospheric static stability. We note that the cloud wave simultaneously detected in the ultraviolet and near infrared images corresponds to one of the two cases of long vertical wavelengths. The lower cloud waves (Figure 5b) are more abundant and are homogeneously distributed in the plot in regions of short vertical wavelengths (5–10 km). This is coherent with the vertical extent of the duct and consistent with the fact that more vertically extended waves would be dispersed by the interaction with the vertical wind shear [*Leroy and Ingersoll*, 1995].

[24] In both cases, phase velocities relative to the mean zonal flow are low, as one would expect, for convectively driven gravity waves typically have small phase speeds relative to the mean zonal wind where they are generated. Also the observed nondispersive behavior of the waves is easily explained by Figure 5 and points to relatively small variations of the vertical wavelength and vertical stability variations across the wave packet extending several hundred kilometers.

[25] Although a full nonlinear approach is beyond the scope of this paper we note that in the limit $|c - u| \rightarrow 0$ the waves encounter a critical level where linearity does not hold and the waves break in the atmosphere. The more slowly traveling waves on Venus are therefore close to the critical level (but not breaking since we are able to observe them for 1–2 h in the VIRTIS frames of the same atmospheric area). Notably under the WKB approximation, as the critical level is approached the vertical wavelength diminishes and finally collapses. However, the wave stalls and the limit is only reached after a time that approaches infinite [*Salby*, 1996]. This process is accompanied by an increase of the wave amplitude. For the IR waves in our survey it seems that the better they can be seen the slower the phase velocities they have, what might be a signature of high-amplitude waves moving close to their critical level.

[26] For the lower cloud waves we can study the double dependence of the phase speed on the two unknowns N^2 (constrained from measurements from previous spacecrafts) and λ_z (constrained by using physically reasonable arguments). This is not feasible on the upper cloud with less observations and apparently larger variations on λ_z or N^2. Figure 6 shows a plot of the total χ^2 deviation of the phase speeds of the waves from the predictions by the wave dispersion relation (equation (2a)). This was calculated for different values of N^2 and λ_z using the equation below which also considers the estimated error in phase speeds determination.

$$\chi^2(N^2, m) = \sum_i^N \left(\frac{c'_x - c_x(N^2, m)}{\sigma_c} \right)^2, \qquad (3)$$

where the index i runs for all of the wave system measured, c'_x is the measured phase speed, c_x is the theoretical value from equation (2a) and σ_c is the variance of the measured phase speeds.

[27] The contours of constant $\Delta\chi^2$ around its minimum value can be used to determine *confidence regions* in the values of the varying parameters N^2 and λ_z. A confidence region is a region within the space of parameters that contains a large percentage of the probability distribution of finding the true parameter values within it [*Press at al.*, 1992]. If all the wave systems measured had the same values of N^2 and λ_z, and measurement errors obeyed a

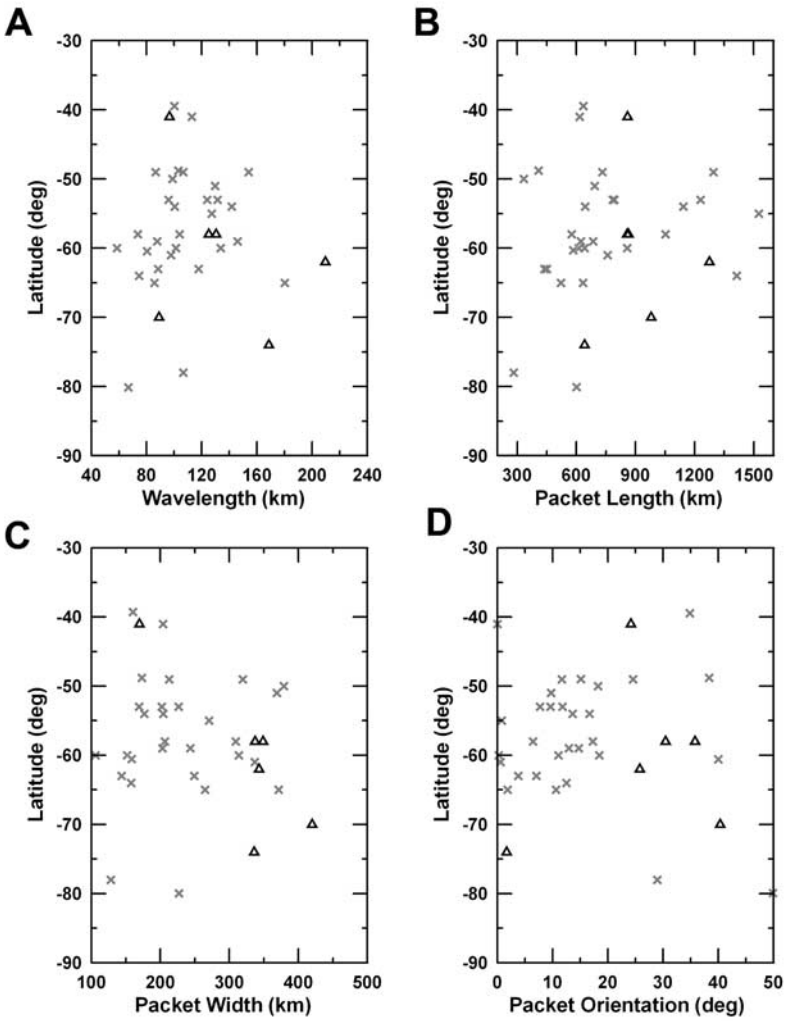

Figure 4. Wave properties in terms of latitude. Figures 4a, 4b, 4c, and 4d show the wavelength, wave packet longitudinal extent, wave packet latitudinal extent, and the wave packet orientation relative to the parallels, respectively. Gravity waves at the upper and lower cloud level are displayed as triangles and crosses, respectively.

normal error distribution, the region surrounded by the $\chi^2 = 2$ curves would have a 68% probability of containing the right values of N^2 and λ_z. The more extended regions surrounded by the $\chi^2 = 5$ and $\chi^2 = 10$ curves would have a 90 and 95% probability of containing the real values. From Figure 6 it seems that, when fixing N^2 with the value introduced previously ($N^2 = 65 \cdot 10^{-6}$ s^{-2}), the confidence region with the best fit between experiment and theory limits the range of vertical wavelengths λ_z between 2 and 5 km (consistent with Figure 5b). This range of vertical wavelengths matches the values of 2.5 km found from temperature scintillations measured by Magellan above the middle cloud deck [*Hinson and Jenkins*, 1995]. These vertically short waves have vertical wave numbers m much larger than the horizontal wave numbers k and equation (2a) can be further simplified to

$$c_x \approx \pm \frac{N}{m}, \tag{4}$$

which results in nondispersive horizontally traveling waves in accordance with the observations.

[28] Convection seems the most plausible source of gravity waves in the lower atmosphere of Venus [*Gierasch et al.*, 1997]. The possibility of internal gravity waves generated by penetrative convection has been previously considered in the terrestrial case [*Stull*, 1976], and it has been extensively studied in Venus through several theoretical and numerical works [*Leroy and Ingersoll*, 1995; *Baker et al.*, 1998, 2000a, 2000b; *Yamamoto*, 2003; *McGouldrick and Toon*, 2008; *Baker et al.*, 1998] which showed that compressible convection in the Venus atmosphere can lead to a significant penetration of the stable layer between 30 and 48 km both by upward convective movements from the unstable layer between 20 and 30 km, and by downward convective movements from the unstable layer between 48 and 55 km. They also pointed out the possibility that the latter convective downwellings could also affect the stable region above 55 km via convective entrainment. *Baker et al.* [2000b] showed that this mechanism works better

producing enhanced overshooting of the convection in regions with high vertical wind shear, which may allow the interaction of upward and downward plumes within the 30–48 km stable layer and generate gravity waves of higher wavelengths. In that case we could anticipate a certain degree of correlation between the locations of gravity waves in the upper and lower clouds. Unfortunately the scarce gravity waves observed in the upper cloud layer may not be enough to closely examine this issue. Also, since the lower clouds are observed in the nightside hemisphere and the upper cloud are observed in the dayside hemisphere, our VIRTIS observations do not cover the same locations in high resolution and close in time.

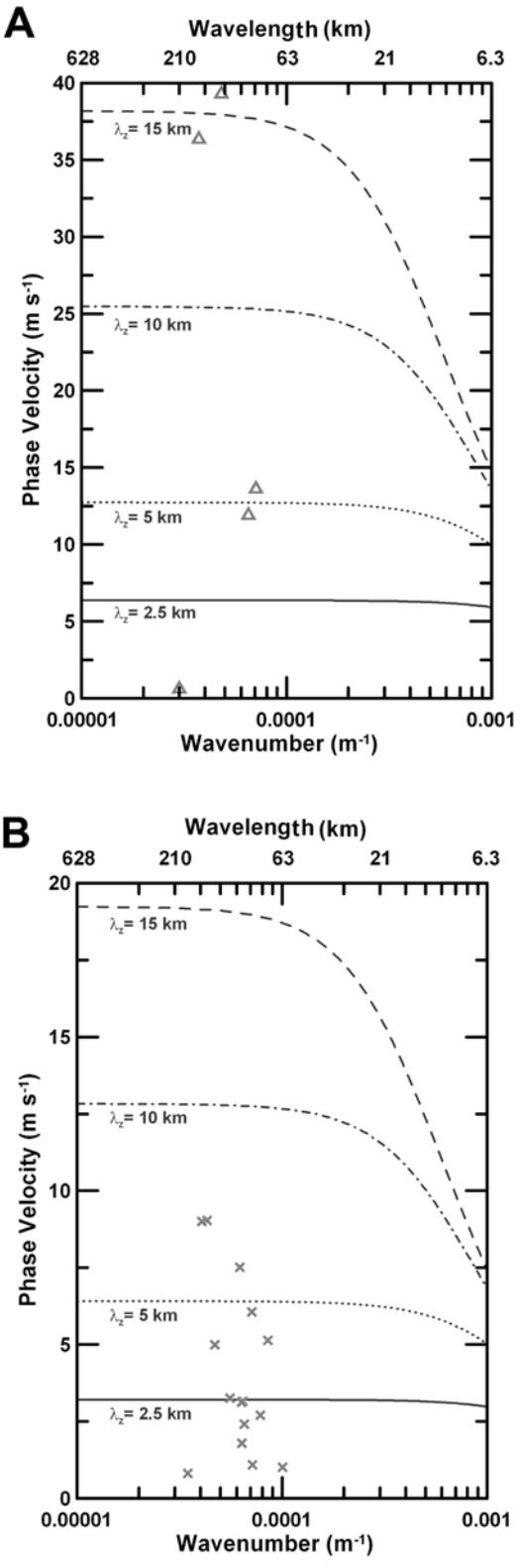

Figure 5. Internal gravity wave dispersion relation applied to the cloud waves in the (a) upper cloud and (b) lower cloud. Phase velocities are relative to the zonal wind. Lines represent solutions to equation (2a) varying the vertical wavelengths in the ranges λ_z = 2–15 km for both clouds. We used a fixed value of the buoyancy frequency representative of the two cloud levels ($N^2 = 260 \cdot 10^{-6}$ s^{-2} for the upper cloud and $N^2 = 65 \cdot 10^{-6}$ s^{-2} for the lower cloud; details are given in section 4).

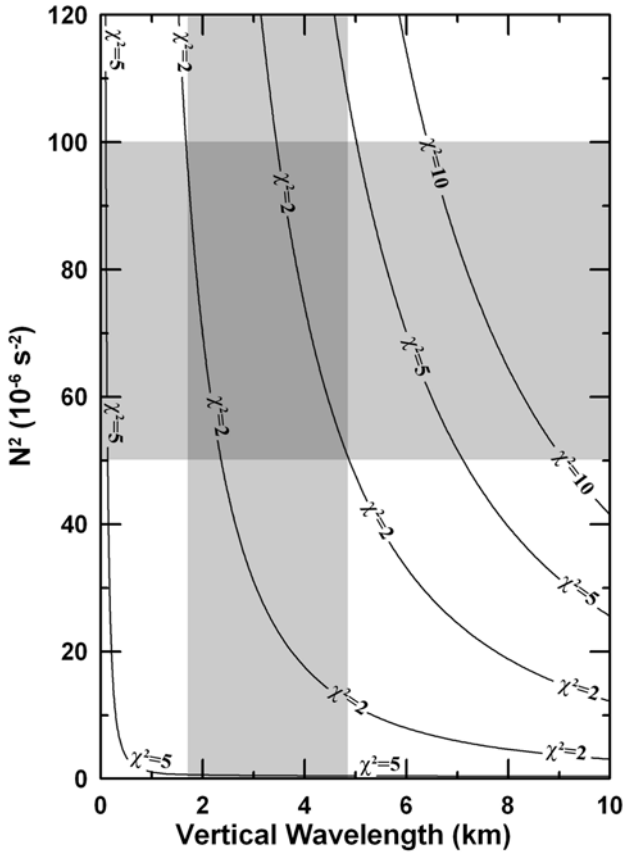

Figure 6. Chi-square tests exploring the space parameter defined by equation (2a) on the lower cloud waves. Confidence regions corresponding to values of chi-square larger than a given value are displayed with contour lines. The horizontal gray area indicates the range of possible buoyancy frequencies at the cloud waves' location, and the vertical gray area indicates the corresponding range of vertical wavelengths within the confidence region of the best fit (bounded by $\chi^2 = 2$ lines).

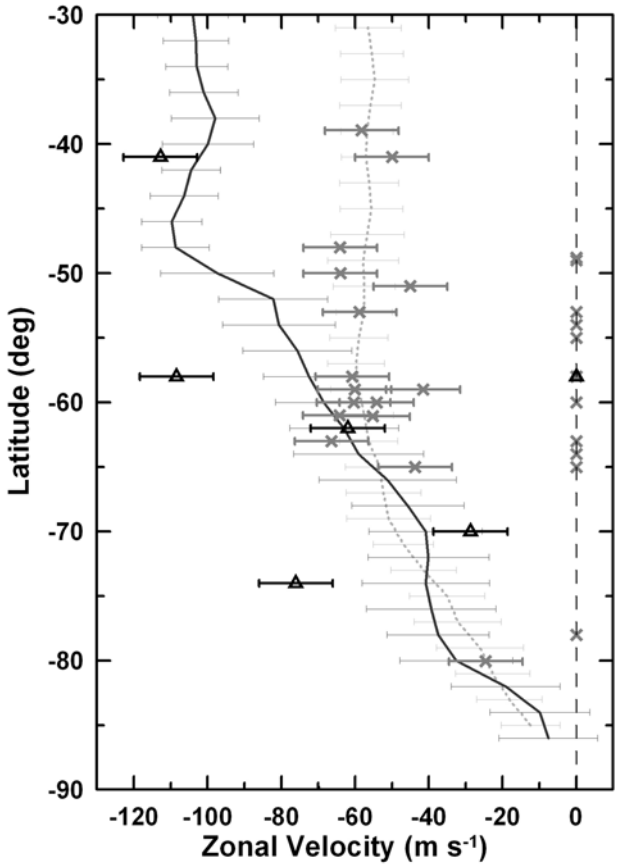

Figure 7. Waves' phase velocity and mean zonal wind profiles at the two cloud levels. Wave phase velocities and the mean zonal wind profile at the upper cloud level are displayed with dark triangles and continuous line. Wave phase velocities and the mean zonal wind profile at the lower cloud level are displayed with light crosses and discontinuous line. Those waves with no dynamical information are also displayed along a discontinuous line at zero zonal velocity. The error bars in the zonal wind profiles represent measurement errors and variance of the wind at each latitude [*Sánchez-Lavega et al.*, 2008]; the error bars of the wave phases represent estimated measurement error in each wave packet.

[29] Our observations, coupled to data from previous spacecraft probes that extend in time and cover ample locations (Pioneer-Venus, Venera and Vega landers, see, e.g., *Gierasch et al.* [1997]), suggests that the presence of the two stable layers where the clouds lie are a persistent feature of Venus's vertical cloud structure. Our gravity wave detections in the south hemisphere from latitudes 40°S to 75°S imply that the layer sampled with infrared images favors the vertical stability. The region equatorward of 40°S is not sampled well enough to extend this conclusion and could be dominated by stronger convective motions, whereas poleward of 75° the dipole feature may mask the presence of the waves. Although abundant and recurrent, the waves observed in the lower cloud are not permanent. In view of the stability measurements obtained from the different previous probes we interpret this variability as a perturbation distinct to changes in the atmospheric stability and affecting the mechanisms responsible of exciting the waves.

[30] The relation between wave location and wind is examined in Figure 7. Here we show the zonal wind profiles in the upper and lower cloud layers obtained by extensive analysis of the VIRTIS data set [*Sánchez-Lavega et al.*, 2008] compared to the zonal phase speeds of the wave systems in both levels. The position of the waves is correlated neither with changes in the zonal profile, nor with values of the vertical wind shear. Additionally, the width of the wave packets does not correlate with the meridional shear of the wind, what may imply that the packet width could be related with meridional variations in the atmospheric static stability.

[31] The significantly larger phase speeds of the waves in the upper cloud is probably a consequence of the stronger stability in this cloud level, with much higher values for the buoyancy frequency [*Seiff et al.*, 1985; *Gierasch et al.*, 1997]. Contrary to the lower cloud waves, which are vertically confined in a duct of static stability, these upper cloud waves are not bounded vertically. This may result in vertical propagation to levels where they are critically absorbed by the vertically varying mean flow, or dissipated [*Schubert and Walterscheid*, 1984]. The absorbed waves transport energy and momentum. Their role in powering the atmospheric superrotation was examined by *Leroy and Ingersoll* [1995] who concluded that the waves are probably not responsible for the atmospheric global winds.

[32] Most of the numerical studies of gravity waves on Venus focus on waves of smaller wavelengths (no larger than 30 km, see *Baker et al.* [1998, 2000a, 2000b]) than those here reported (typically 100 km). While our observations cannot distinguish these high-frequency waves (our best resolution images have a pixel size of 15–20 km) we do detect significant wave activity of larger wavelengths (100 km). *McGouldrick and Toon* [2008] suggest that gravity waves with greater horizontal wavelengths comparable to our observations could be generated by broad convective plumes or a large magnitude of the vertical shear of the zonal wind but we do not observe significant convection on the upper or lower clouds. The vertical wind shear of the wind from VIRTIS data is mainly confined to the 61 to 66 km altitude range with values $\partial < u > /\partial z = 8 \pm 2$ ms^{-1} per km at equatorial to midlatitudes and less than 2 ms^{-1} per km at subpolar latitudes [*Sánchez-Lavega et al.*, 2008].

[33] Gravity waves transmit energy and momentum perpendicularly to the direction of phase propagation in the direction of constant phase lines (considering the traveling direction, mainly zonal, and the vertical). Most of the waves are zonally aligned but some others are tilted and may transport some momentum meridionally. In the zonal direction some of the waves move slightly faster while others slightly more slowly than the average wind. In the meridional direction some waves move slightly northward and some other slightly southward. We also do not have information about the vertical component of the wave motion. For these reasons it was difficult to evaluate the

average role of the waves in the global transport of energy and momentum in the atmosphere.

5. Conclusions

[34] We have presented a study of the mesoscale waves present in the atmosphere of Venus at different cloud levels by using images at three wavelengths obtained by the VIRTIS instrument onboard Venus Express. We interpret them as gravity waves, and this is the first time that mesoscale waves within three different cloud levels are characterized in Venus at the same time, these levels corresponding to wavelengths 380 nm, 980 nm, and 1.74 μm.

[35] The abundant waves observed in IR images display a large diversity of morphologies and wave properties with many observations revealing wave activity at a wide range of latitudes (40°S–75°S). None of the wave properties seem to vary systematically with latitude or the zonal wind profile except from an observational bias of the VIRTIS data set that is unable to observe these waves at tropical and equatorial latitudes. In particular the location of the waves seems uncorrelated with topographic features on the surface or the local time that combined with the negligible effect of the solar heating at the lower cloud could indicate a crucial role of deep convection as the source of wave activity.

[36] We have presented a first account on wave properties using a classical "textbook" linear model of gravity waves [*Holton*, 1992] that confirms the nature of the waves. From our statistical analysis of the wave dependence on the static stability and vertical wavelength (Figures 5b and 6) we concluded that the vertical wavelengths are on the order of 2 to 5 km in the lower cloud and 5 to 15 km in the upper cloud from the less numerous measurements of wavelength and phase speeds (Figure 5a). These results are consistent with previous determinations of the vertical wavelengths of temperature scintillations in the middle cloud measured by the Magellan spacecraft [*Hinson and Jenkins*, 1995].

[37] This study opens questions about the specific source of the wave activity observed, the latitudinal and temporal distributions of atmospheric stability and convection and the role of these waves in the overall dynamics of Venus atmosphere.

[38] **Acknowledgments.** This work has been funded by Spanish MEC AYA2006-07735 with FEDER support and Grupos Gobierno Vasco IT-464-07. J.P. acknowledges a UPV fellowship, and R.H. acknowledges a "Ramón y Cajal" contract from MEC.

References

Baker, R. D., G. Schubert, and P. W. Jones (1998), Cloud-level penetrative compressible convection in the Venus atmosphere, *J. Atmos. Sci.*, *55*, 3–18, doi:10.1175/1520-0469 (1998)055<0003:CLPCCI>2.0.CO;2.

Baker, R. D., G. Schubert, and P. W. Jones (2000a), Convectively generated inertial gravity waves in the lower atmosphere of Venus. Part I: No wind shear, *J. Atmos. Sci.*, *57*, 184–199, doi:10.1175/1520-0469(2000)057<0184:CGIGWI>2.0.CO;2.

Baker, R. D., G. Schubert, and P. W. Jones (2000b), Convectively generated inertial gravity waves in the lower atmosphere of Venus. Part II: Mean wind shear and wave-mean flow interaction, *J. Atmos. Sci.*, *57*, 200–215, doi:10.1175/1520-0469(2000)057<0200:CGIGWI>2.0.CO;2.

Belton, M. J. S., G. R. Smith, G. Schubert, and A. D. Del Genio (1976), Cloud patterns, waves and convection in the Venus atmosphere, *J. Atmos. Sci.*, *33*, 1394–1417, doi:10.1175/1520-0469(1976)033<1394:CPWACI>2.0.CO;2.

Belton, M. J. S., et al. (1991), Images from Galileo of the Venus cloud deck, *Science*, *253*, 1531–1536, doi:10.1126/science.253.5027.1531.

Carlson, R. W., K. H. Baines, L. W. Kamp, P. R. Weissman, W. D. Smythe, A. C. Ocampo, T. V. Johnson, D. L. Matson, J. B. Pollack, and D. Grinspoon (1991), Galileo infrared imaging spectroscopy measurements at Venus, *Science*, *253*, 1541–1548, doi:10.1126/science.253.5027.1541.

Counselman, C. C., S. A. Gourevitch, R. W. King, G. B. Loriot, and E. S. Ginsberg (1980), Zonal and meridional circulation of the lower atmosphere of Venus determined by radio interferometry, *J. Geophys. Res.*, *85*, 8026–8030, doi:10.1029/JA085iA13p08026.

Crisp, D., S. McMuldroch, S. K. Stephens, W. M. Sinton, B. Ragent, K. W. Hodapp, R. G. Probst, L. R. Doyle, D. A. Allen, and J. Elias (1991), Ground-based near-infrared imaging observations of Venus during the Galileo encounter, *Science*, *253*, 1538–1541, doi:10.1126/science.253.5027.1538.

Del Genio, A. D., and W. B. Rossow (1990), Planetary-scale waves and the cyclic nature of the cloud top dynamics on Venus, *J. Atmos. Sci.*, *47*, 293–318, doi:10.1175/1520-0469(1990)047<0293:PSWATC>2.0.CO;2.

Drossart, P., et al. (2007), Scientific goals for the observation of Venus by VIRTIS on ESA/Venus express mission, *Planet. Space Sci.*, *55*, 1653–1672, doi:10.1016/j.pss.2007.01.003.

Esposito, L. W., J. L. Bertaux, V. Krasnopolsky, V. I. Moroz, and L. V. Zasova (1997), Chemistry of lower atmosphere and clouds, in *VENUS II: Geology, Geophysics, Atmosphere, and Solar Wind Environment*, pp. 415–458, Univ. of Ariz. Press, Tucson.

Flasar, F. M., and P. J. Gierasch (1986), Mesoscale waves as a probe of Jupiter's deep atmosphere, *J. Atmos. Sci.*, *43*, 2683–2707, doi:10.1175/1520-0469(1986)043<2683:MWAAPO>2.0.CO;2.

Gierasch, P. J. (1987), Waves in the atmosphere of Venus, *Nature*, *328*, 510–512, doi:10.1038/328510a0.

Gierasch, P. J., et al. (1997), The general circulation of the Venus atmosphere: An assessment, in *VENUS II: Geology, Geophysics, Atmosphere, and Solar Wind Environment*, pp. 459–500, Univ. of Ariz. Press, Tucson.

Hinson, D. P., and J. M. Jenkins (1995), Magellan radio occultation measurements of atmospheric waves on Venus, *Icarus*, *114*(2), 310–327, doi:10.1006/icar.1995.1064.

Holton, J. R. (1992), *An Introduction to Dynamic Meteorology*, 535 pp., Elsevier, New York.

Hou, A. Y., and B. F. Farrell (1987), Superrotation induced by critical-level absorption of gravity waves on Venus: An assessment, *J. Atmos. Sci.*, *44*, 1049–1061, doi:10.1175/1520-0469(1987)044<1049:SIBCLA>2.0.CO;2.

Houze, R. A. (1993), *Cloud Dynamics*, 573 pp., Elsevier, New York.

Hunt, G. E., and J. P. Muller (1979), Voyager observations of small-scale waves in the equatorial region of the jovian atmosphere, *Nature*, *280*, 778–780, doi:10.1038/280778a0.

Kasprzak, W. T., A. E. Hedin, H. G. Mayr, and H. B. Niemann (1988), Wavelike perturbations observed in the neutral thermosphere of Venus, *J. Geophys. Res.*, *93*, 11,237–11,245, doi:10.1029/JA093iA10p11237.

Kliore, A. J., and I. R. Patel (1980), Vertical structure of the atmosphere of Venus from Pioneer Venus orbiter radio occultations, *J. Geophys. Res.*, *85*, 7957–7962, doi:10.1029/JA085iA13p07957.

Kolosov, M. A., O. I. Yakovlev, A. I. Efimov, S. S. Matyugov, T. S. Timofeeva, E. V. Chub, A. G. Pavelyev, A. I. Kucheryavenkov, I. E. Kalashnikov, and O. E. Milekhin (1980), Investigation of the Venus atmosphere and surface by the method of radiosounding using VENERA-9 and 10 satellites, *Acta Astronaut.*, *7*, 219–234, doi:10.1016/0094-5765(80)90062-4.

Leroy, S. S., and A. P. Ingersoll (1995), Convective generation of gravity waves in Venus's atmosphere: Gravity wave spectrum and momentum transport, *J. Atmos. Sci.*, *52*, 3717–3737, doi:10.1175/1520-0469(1995)052<3717:CGOGWI>2.0.CO;2.

Leroy, S. S., and A. P. Ingersoll (1996), Radio scintillations in Venus's atmosphere: Application of a theory of gravity wave generation, *J. Atmos. Sci.*, *53*, 1018–1028, doi:10.1175/1520-0469(1996)053<1018:RSIVAA>2.0.CO;2.

Markiewicz, W. J., D. V. Titov, S. S. Limaye, H. U. Keller, N. Ignatiev, R. Jaumann, N. Thomas, H. Michalik, R. Moissl, and P. Russo (2007), Morphology and dynamics of the upper cloud layer of Venus, *Nature*, *450*, 633–636, doi:10.1038/nature06320.

McGouldrick, K., and O. B. Toon (2008), Observable effects of convection and gravity waves on the Venus condensational cloud, *Planet. Space Sci.*, *56*, 1112–1131, doi:10.1016/j.pss.2008.02.010.

Niemann, H. B., W. T. Kasprzak, A. E. Hedin, D. M. Hunten, and N. W. Spencer (1980), Mass spectrometric measurements of the neutral gas composition of the thermosphere and exosphere of Venus, *J. Geophys. Res.*, *85*, 7817–7827, doi:10.1029/JA085iA13p07817.

Peralta, J., R. Hueso, and A. Sánchez-Lavega (2007a), Cloud brightness distribution and turbulence in Venus using Galileo violet images, *Icarus*, *188*, 305–314, doi:10.1016/j.icarus.2006.12.005.

Peralta, J., R. Hueso, and A. Sánchez-Lavega (2007b), A reanalysis of Venus winds at two cloud levels from Galileo SSI images, *Icarus*, *190*, 469–477, doi:10.1016/j.icarus.2007.03.028.

Piccioni, G., et al. (2007), South-polar features on Venus similar to those near the north pole, *Nature*, *450*, 637–640, doi:10.1038/nature06209.

Press, W. H., S. A. Teukolsky, W. T. Vetterling, and B. P. Flannery (1992), *Numerical Recipes in Fortran 77: The Art of Scientific Computing*, pp. 687–693, Cambridge Univ. Press, New York.

Reuter, D. C., et al. (2007), Jupiter cloud composition, stratification, convection and wave motion: A view from New Horizons, *Science*, *318*, 223–225, doi:10.1126/science.1147618.

Rossow, W. B., et al. (1980), Cloud morphology and motions from Pioneer Venus images, *J. Geophys. Res.*, *85*, 8107–8128, doi:10.1029/JA085iA13p08107.

Sagdeev, R. Z., V. M. Linkin, J. E. Blamont, and R. A. Preston (1986), The VEGA Venus balloon experiment, *Nature*, *328*, 510–512.

Salby, M. L. (1996), *Fundamentals of Atmospheric Physics*, 627 pp., Elsevier, New York.

Sánchez-Lavega, A., et al. (2008), Variable winds on Venus mapped in three dimensions, *Geophys. Res. Lett.*, *35*, L13204, doi:10.1029/2008GL033817.

Saunders, R. S., R. E. Arvidson, J. W. Head III, G. G. Schaber, E. R. Stofan, and S. C. Solomon (1991), An overview of Venus geology, *Science*, *252*, 249–252, doi:10.1126/science.252.5003.249.

Schubert, G. (1983), General circulation and the dynamical state of the Venus, in *VENUS*, pp. 681–765, Univ. of Ariz. Press, Tucson.

Schubert, G., and R. L. Walterscheid (1984), Propagation of small-scale acoustic-gravity waves in the Venus atmosphere, *J. Atmos. Sci.*, *41*, 1202–1213.

Seiff, A., D. B. Kirk, R. E. Young, R. C. Blanchard, J. T. Findlay, G. M. Kelly, and S. C. Sommer (1980), Measurements of thermal structure and thermal contrasts in the atmosphere of Venus and related dynamical observations: Results from the four Pioneer Venus probes, *J. Geophys. Res.*, *85*, 7903–7933, doi:10.1029/JA085iA13p07903.

Seiff, A., J. T. Schofield, A. J. Kliore, F. W. Taylor, S. S. Limaye, H. E. Revercomb, L. A. Sromovsky, V. V. Kerzhanovich, V. I. Moroz, and M. Y. Marov (1985), Models of the structure of the atmosphere of Venus from the surface to 100 kilometers altitude, *Adv. Space Res.*, *5*(11), 3–58, doi:10.1016/0273-1177(85)90197-8.

Stull, R. B. (1976), Internal gravity waves generated by penetrative convection, *J. Atmos. Sci.*, *33*, 1279–1286, doi:10.1175/1520-0469(1976)033<1279:IGWGBP>2.0.CO;2.

Svedhem, H., et al. (2007), Venus Express: The first European mission to Venus, *Planet. Space Sci.*, *55*, 1636–1652, doi:10.1016/j.pss.2007.01.013.

Taylor, F. W., et al. (1980), Structure and meteorology of the middle atmosphere of Venus: Infrared remote sensing From the Pioneer Orbiter, *J. Geophys. Res.*, *85*, 7963–8006, doi:10.1029/JA085iA13p07963.

Toigo, A., P. J. Gierasch, and M. D. Smith (1994), High resolution cloud feature tracking on Venus by Galileo, *Icarus*, *109*, 318–336, doi:10.1006/icar.1994.1097.

Yamamoto, M. (2003), Gravity waves and convection cells resulting from feedback heating of Venus' lower clouds, *J. Meteorol. Soc. Jpn.*, *81*, 885–892, doi:10.2151/jmsj.81.885.

Young, R. E., R. L. Walterscheid, G. Schubert, A. Seiff, V. M. Linkin, and A. N. Lipatov (1987), Characteristics of gravity waves generated by surface topography on Venus: Comparison with the VEGA balloon results, *J. Atmos. Sci.*, *44*, 2628–2639, doi:10.1175/1520-0469(1987)044<2628:COGWGB>2.0.CO;2.

Young, R. E., R. L. Walterscheid, G. Schubert, L. Pfister, H. Houben, and D. L. Bindschadler (1994), Characteristics of finite amplitude stationary gravity waves in the atmosphere of Venus, *J. Atmos. Sci.*, *51*, 1857–1875, doi:10.1175/1520-0469(1994)051<1857:COFASG>2.0.CO;2.

P. Drossart, Observatoire de Paris, LESIA, 5 place Jules Janssen, F-92195 Meudon, France.

R. Hueso, J. Peralta, and A. Sánchez-Lavega, Departamento de Física Aplicada I, Escuela Técnica Superior de Ingenieríos, Universidad del País Vasco, Alameda Urquijo s/n, E-48013, Bilbao, Spain. (javier.peralta@ehu.es)

G. Piccioni and O. Lanciano, Istituto di Astrofisica Spaziale e Fisica Cosmica, INAF, via del Fosso del Cavaliere 100, I-00133 Rome, Italy.